Presented at the 35th PVSC, June 20-25, 2010, Honolulu, Hawaii

n-TYPE SILICON – ENABLING EFFICIENCIES > 20% IN INDUSTRIAL PRODUCTION

S. W. Glunz, J. Benick, D. Biro, M. Bivour, M. Hermle, D. Pysch, M. Rauer,
C. Reichel, A. Richter, M. Rüdiger, C. Schmiga, D. Suwito, A. Wolf, R. Preu
Fraunhofer Institute for Solar Energy Systems (ISE), Heidenhofstr. 2, 79110 Freiburg, Germany
Corresponding author: Stefan Glunz, Phone: +49-761-4588-5191, email: stefan.glunz@ise.fraunhofer.de

ABSTRACT

In the first part of this paper we estimate the efficiency potential of crystalline silicon solar cells on conventionally pulled *p*-type boron-doped Czochralski-grown silicon with typical oxygen concentrations. Taking into account an industrial high-efficiency cell structure featuring fine-line metallization, shallow and well-passivated emitter and a rear surface structure with dielectric passivation and local laser-fired point contacts, the maximum achievable efficiency is around 20%. The main limitation of such a cell is due to the rather low bulk lifetime after light-induced degradation. Even when avoiding the metastable boron-oxygen defect by using Gallium-doped or magnetic Cz-silicon, it has to be kept in mind that the detrimental impact of metal contaminations on *p*-type silicon is greater than on *n*-type silicon. A potential strategy to reduce this loss is the use of *n*-type silicon. Therefore, the second part of the paper discusses different architectures for solar cells on *n*-type silicon substrates and shows the latest results achieved at Fraunhofer ISE in this field.

INTRODUCTION

Currently numerous equipment suppliers and solar cell manufactures are focusing on improvements of the front side of silicon solar cells as the introduction of selective emitters or advanced metallization. This is a reasonable trend since the optimization of the front side structure resulting in (i) better blue response, (ii) reduced shadowing loss, (iii) decreased resistive losses, and (iv) lower emitter dark saturation current will yield a significant efficiency gain for all silicon qualities even for material with diffusion lengths in the range or even lower than cell thickness. It can be estimated that depending on the quality of the applied improvement a gain in efficiency of about 0.5%$_{abs}$ to 1%$_{abs}$ can be achieved. Figure 1 shows the efficiency gains by different improvements comparing a 16.6% with a 22.4% efficient solar cell. While the improvement on the front side (reduced series resistance, labeled "R_s", and reflection and shadowing loss, labeled "Reflection", lower J_{oe} and improved blue response, labeled "Emitter and front surface") are significant, it is important to utilize the efficiency potential related to improvements in the bulk ("Bulk recombination") and at rear surface ("Rear surface").

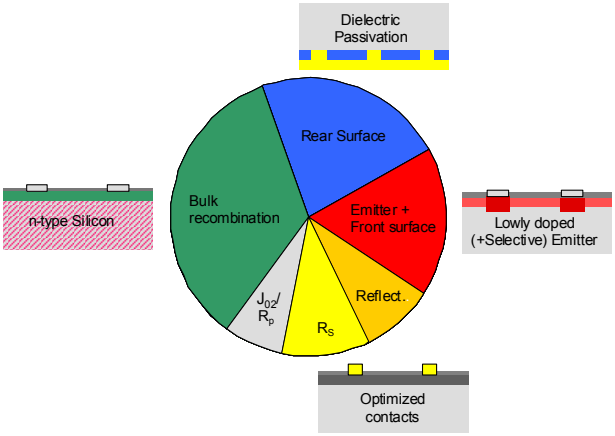

Figure 1 Efficiency gain achieved by different improvements. The model calculation compares a cell with 16.6% efficiency with a high-efficiency cell with 22.4% efficiency.

Dielectric passivation layers and locally defined rear contacts can reduce the surface recombination velocity to effective values around 100 cm/s and additionally increase the internal reflectivity. While the latter improvement will help to increase the efficiency even on low-quality material, the full improvement – especially a gain in open-circuit voltage – will only be accessible with reasonable material quality. The standard monocrystalline industrial material, i.e. boron-doped *p*-type Cz-silicon, suffers from light-induced degradation [1-3] which restricts the lifetime to a fundamental limit. Additionally, the detrimental impact of metal contaminations on *p*-type silicon is greater than on *n*-type silicon [4]. Therefore, in the first part of the paper we will estimate the maximum achievable efficiency on this material type. The second part gives an overview about cell structures on *n*-type silicon investigated at Fraunhofer ISE.

EFFICIENCY POTENTIAL ON BORON-DOPED CZ-SILICON

In order to calculate the efficiency potential on boron-doped Cz-silicon we have assumed a high-efficiency cell PERC[5]/LFC[6] structure with a well-passivated emitter and advanced metallization, keeping in mind that the cell process should be still industrially feasible. The following table gives details of the chosen parameters.

Table 1: Parameters used for model calculation

Parameter	Value
Shadow loss due to front metallization	5%
Recombination in emitter, J_{0e}	100 fA/cm^2 (--> $V_{oc,max}$ ~ 685 mV)
Maximum achievable *FF* due to J_{02} and R_p, *PFF*	~ 82.5%
Bulk recombination due to boron-oxygen complex, τ_{CZ}	Fundamental limit given by Bothe et al.[7] with a factor of 2 due to improvements by high-temperature steps [2, 7]
Residual SRH bulk recombination due to metal contamination, τ_{metal}	1000 µs
Intrinsic bulk recombination (Auger and direct), τ_{intr}	Doping-dependent parameterization [8]
Base resistivity, ρ_{base}	Variation between 0.1 and 10 Ω cm
Oxygen concentration, O_i	0 and 6 - 9x10^{17} cm^{-3}
Surface recombination velocity at rear dielectric layer, S_{pass}	Doping dependent parameterization for alnealed thermally grown oxide [9]
Surface recombination velocity at laser-fired metal contact points, S_{met}	Doping dependent parameterization for laser-fired contacts [10]
Effective surface recombination velocity at rear surface, S_{eff}	Calculation using S_{met} and S_{pass} with Fischer equation [11]
Effective base resistance, R_{base}	Spreading resistance calculation using Cox and Strack [12]
Distance of rear point contacts	Optimum distance calculated for each base doping using Pitchmaster software [13]
Additional series resistance due to metallisation and emitter, $R_{s,residual}$	0.3 Ω cm^2

Since we have chosen a high lifetime due to metal contamination τ_{metal}, the limiting factor of the base material is the bulk recombination via the metastable oxygen-boron defect. Bothe *et al.* [7] have given a fundamental limit of the lifetime in the degraded state as a function of oxygen and boron concentration. It is important to note that this lifetime is valid for unprocessed wafer. In several publications [2, 7] it was reported that the concentration of the metastable defect is reduced by a factor of 2 to 3 by high-temperature steps above 700°C. Since this is the case for our cell process (emitter diffusion, …) we have assumed the fundamental lifetime limit of Bothe *et al.* multiplied by a factor of 2:

$$\tau_{Cz} = 2 \times 7.675 \times 10^{45} \left[B_s\right]^{-0.824} \left[O_i\right]^{-1.748} \qquad (1)$$

For our calculations we have chosen typical oxygen concentrations between 6 and 9x10^{17} cm^{-3} and 0 cm^{-3} as a reference. This results in bulk diffusion lengths as shown in Figure 2. The quite dramatic difference of the material with no oxygen content and the ones with realistic concentrations is obvious. At low base resistivities intrinsic recombination channels as Auger recombination are getting importance especially for the ideal material. It has to be kept in mind that we have chosen a very high residual lifetime of 1000 µs. This will be not always easy to achieve under realistic conditions since the lifetime in *p*-type silicon is reduced even by low impurity concentrations due to the asymmetric capture cross sections of most metal impurities [4]. However, it is a valuable case study to evaluate the potential of our cell structure under ideal conditions.

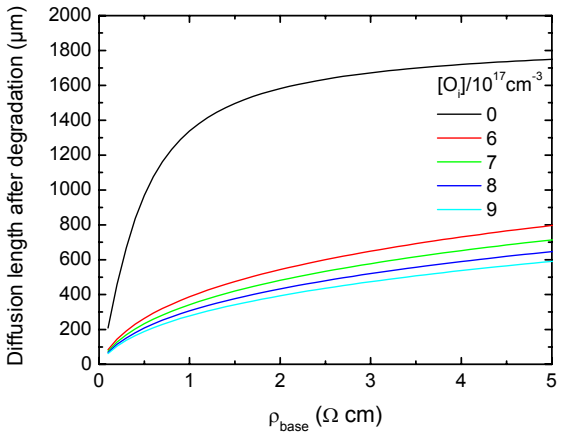

Figure 2 Bulk diffusion length as a function of base resistivity for different oxygen concentrations.

For the rear surface structure we have selected a combination of laser-fired contacts and alnealed thermally grown oxide since this results in very high efficiencies and a doping-dependent parameterisation of the surface recombination velocity is known [9, 10]. For technical reasons i.e. low deposition temperature, it might be preferable to choose Al_2O_3 as rear surface passivation layer. However, that will not change the result of our calculation significantly since from a recent publication [14] it is known that using Al_2O_3 nearly identical cell parameters can be achieved as with thermally grown oxide. The pitch of the point contacts is optimized by the spread-sheet-based software Pitchmaster [13] as a compromise of recombination losses and base spreading resistance. Pitchmaster calculates the cell parameters for the optimum point contact pitch for each individual base doping concentration. The results as function of base resistivity for a cell thickness *W* of 190 µm are given in the following Figures 3-6.

In all cases the short-circuit current increases with increasing base resistivity since the effective diffusion length, L_{eff}, taking into account bulk and rear recombination increases.

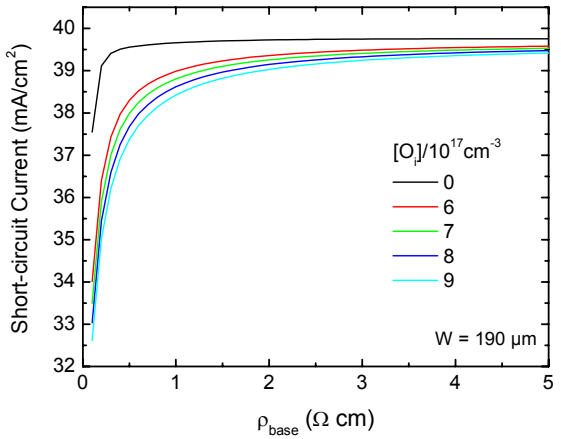

Figure 3 Short-circuit current as a function of base resistivity for different oxygen concentrations. The pitch of the rear contacts was optimized for each base resistivity.

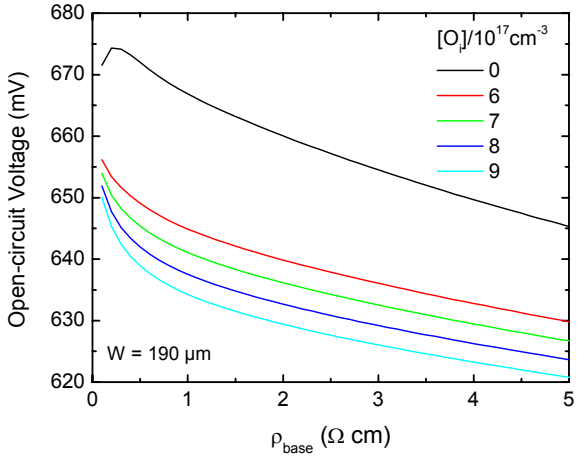

Figure 4 Open-circuit voltage as a function of base resistivity for different oxygen concentrations. The pitch of the rear contacts was optimized for each base resistivity.

However, the open-circuit voltage decreases for increasing base resistivity. This is mainly due to the fact that the doping-dependent reduction of the surface recombination follows an exponential law with an exponent smaller than 1 [10,11]. This is too small to compensate for the doping-dependent increase in J_{0b} following an exponent of -1:

$$J_{0b} \propto n_i^2 / N_A \qquad (2)$$

The fill factor is reduced with increasing base resistivity due to the increasing spreading resistance.

As a result of these three trends the efficiency shows a maximum value which depends on the material quality i.e. oxygen concentration: The higher the material quality, the lower the optimum base resistivity.

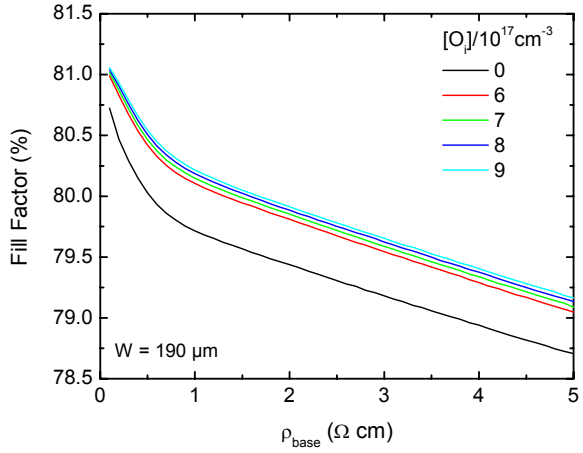

Figure 5 Fill factor as a function of base resistivity for different oxygen concentrations. The pitch of the rear contacts was optimized for each base resistivity

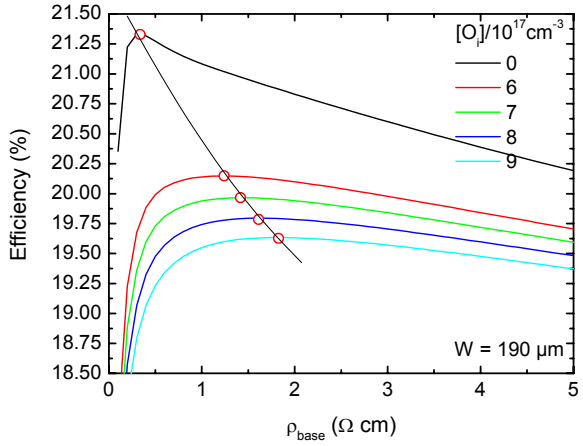

Figure 6 Efficiency as a function of base resistivity for different oxygen concentrations. The maximum efficiencies for each oxygen concentration are denoted by a circle. The pitch of the rear contacts was optimized for each base resistivity.

While the cell structure offers an efficiency potential of more than 21%, the best values for oxygen-contaminated materials are in the range between 19.6% and 20.1% for low and high oxygen concentration, respectively.

In order to reduce the influence of the bulk recombination it is possible to reduce the thickness of the wafer. In fact the maximum efficiency on a 130 µm wafer with oxygen concentration of 6×10^{17} cm^{-3} and remaining the same cell architecture results in an efficiency increase of around 0.2%$_{abs}$. Although the LFC contacts already provide a local Al-BSF, the introduction of a higher doping concentration underneath the local rear contacts as the local boron BSF in PERL cells could increase the efficiency by ~0.3%$_{abs}$.

Other authors [15] have performed similar calculations for PERC structures without local Al-BSF but restricted their simulation to a low base resistivity (0.5 Ω cm) which is necessary for a pure PERC structure without local Al-BSF.

Although the basic trend of their simulation is similar, the restriction to low base resistivity leads to an underestimation of the potential of oxygen-contaminated Cz-silicon which reaches its best efficiencies at higher bulk resistivities. This shows the importance of a proper local back surface field (BSF) not only to increase the quality of the cell structure in general but also to be more flexible in the choice of bulk resistivity.

In conclusion our model calculation shows that for the standard industrial material i.e. oxygen-contaminated boron-doped Cz-silicon the threshold of 20% can be reached but not surpassed significantly. Thus, for the upcoming cell generation this material type is still usable but for future cell developments the material issue has to be tackled.

In order to reduce the impact of the metastable defect, either *p*-type gallium-doped, *p*-type magnetic Cz-silicon (MCz) [16] or the regeneration process [17, 18] could be used. While for gallium-doped silicon the low segregation coefficient of gallium and IP-issues have to be considered, the MCz-route suffers from high Capex-costs. In all three cases, the use of *p*-type silicon results in a low tolerance in respect to most metal contaminations [4]. Therefore the best choice for future cell generations might be *n*-type silicon. In fact both companies achieving efficiencies of more than 20% in industrial production today use *n*-type silicon. However, using *n*-type silicon the cell structure has to be changed significantly. The following chapter discusses several cell architectures and the results obtained at Fraunhofer ISE.

RESULTS ON *n*-TYPE SILICON AT FRAUNHOFER ISE

Aluminum-alloyed back junction

The easiest way to realize a solar cell on *n*-type silicon is to utilize the full-area screen-printed Al-alloyed BSF of standard industrial *p*-type cell structures as the p^+-back junction of *n*-type cells. As effective passivation of the front surface is an important prerequisite for high efficiency of back-junction cells, we have developed a special metallic ink for aerosol-printing of the grid which also allows weakly doped surfaces to be contacted. Even without an additional passivation layer on the rear side high efficiencies of 18.6% on large cells [19] and 19.8% on small cells [20] were achieved.

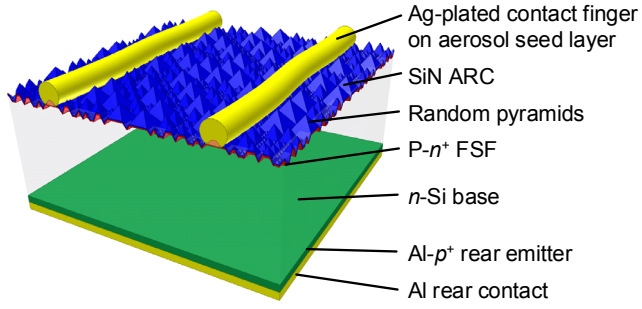

Figure 7 Cell structure with Al-alloyed rear emitter.

By the addition of a passivation layer on the rear emitter surface J_{oe} can be reduced [21] and the internal optical reflectivity increases. In this way, we have already demonstrated efficiencies exceeding 20% [20].

Table 2 Results of cells with Al-alloyed back junction and no additional rear passivation layer. *= Measurements confirmed by Fraunhofer ISE Callab.

Process type	A [cm^2]	V_{oc} [mV]	J_{sc} [mA/cm^2]	FF [%]	η [%]
Industrial	148.5	638	36.9	79.2	18.6*
Laboratory	4.0	642	38.7	79.6	19.8*

Boron-diffused front emitter

The next possibility is to switch from an *np* to *pn*-junction on the front side. The p^+-emitter is generated by boron diffusion. In this case it is necessary to passivate the front side with a thin Al_2O_3 layer [22] with its strong negative built-in charge which reduces effectively the front surface recombination. The rear side of the cell shown in Figure 8 is passivated with a thermally grown oxide and locally diffused phosphorus BSFs.

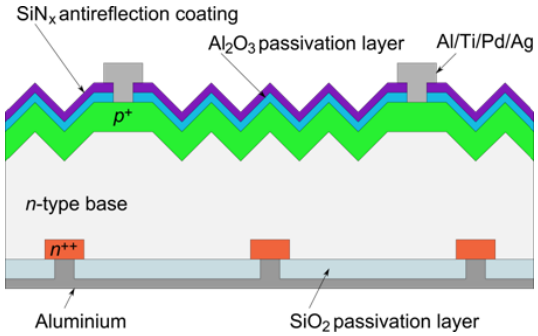

Figure 8 Cell structure with boron-diffused front emitter.

Although this cell has still no selective emitter which gives room for further improvement, recently we have achieved an efficiency of 23.9% [23] for a calibrated aperture area (illuminated area includes bus bar) measurement.

Table 3 Results of cells with boron-diffused front junction (A = 4 cm^2). *= Measurements confirmed by Fraunhofer ISE Callab.

Rear structure	V_{oc} [mV]	J_{sc} [mA/cm^2]	FF [%]	η [%]
Thermal oxide + locally diffused P-BSF	705	41.1	82.5	23.9*
New PassDop layer + laser-fired P-BSF	701	39.8	80.1	22.4*
Full-area P-BSF + printed front contacts	654	38.7	80.8	20.5

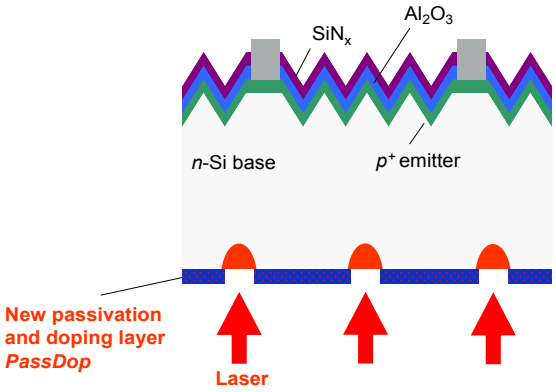

Figure 9 Laser process to create contact openings and local P-BSF using the *PassDop* layer. After this process step an Al-layer is evaporated on the rear surface.

In order to transfer this laboratory cell to an industrial environment several processes have to be simplified. The locally diffused P-BSFs of the lab process using masking oxides and photolithography is too complex for industrial application. Therefore we have developed a new process consisting of two steps: (i) PECVD deposition of phosphorus-containing passivation layer system called *PassDop* and (ii) simultaneous opening of the layer with a laser and generation of local P-BSFs (see Figure 9). Using this new and easy-to-fabricate rear surface process, we were able to achieve a maximum efficiency of 22.4%[24]. The next step for industrialization is the substitution of the evaporated contacts on the front by printed contacts. For the optimization of our printing pastes we have chosen a cell structure with a full-area P-BSF. Even with this simple structure we were able to achieve an efficiency of 20.5% and a FF of 80.8% [25]. In the next step we will combine a printed front side with a dielectrically passivated rear side in order to obtain the full potential of this cell type.

Diffused interdigitated back-junction back-contact

Interdigitated back-junction cells have a very high efficiency potential and are the base structure for the industrial high-efficiency cell A300 by Sunpower [26]. To achieve maximum efficiency, it is important to decouple the structure of the rear metallization of the structure of the diffused regions. While the *p*- and *n*-metallization should have roughly the same area fraction, the area for the *n*-BSF should be restricted to avoid electrical shading [26, 27]. That means that the *n*-metallization fingers overlap the regions with p-emitter (see Figure 10). Therefore, a passivating *and* insulating layer is necessary to avoid any shunting between *n*-finger and *p*-emitter. We have developed a layer system which fulfils these requests and allows the free design of different emitter/BSF patterns as shown in Figure 11 [27].

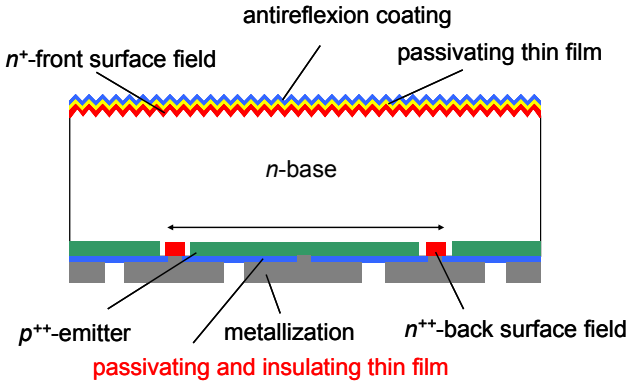

Figure 10 Cell structure with interdigitated boron- and phosphorus-diffused rear structure. A passivating and insulating layer covers the rear surface.

While the pattern in Figure 11a) has the advantage of a high collection probability since nearly the full surface is covered with emitter, the pattern in Figure 11b) reduces the J_0 due to diffused areas and should increase the voltage if the surface passivation at the rear surface works effectively.

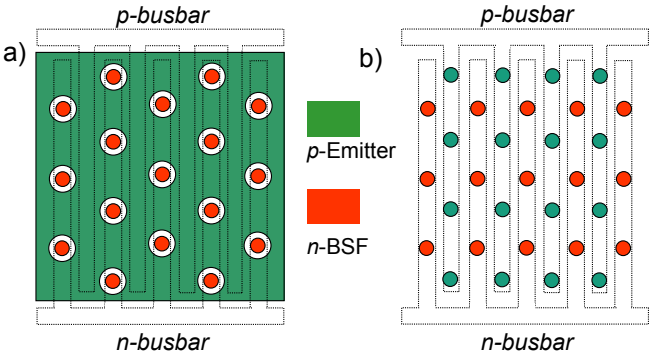

Figure 11 Interdigitated back junction cells with different emitter coverage (not to scale).

In fact the second cell structure results in very high voltages of more than 700 mV which proves the passivation quality of our new layer system [27].

Table 4 Results of cells with interdigitated back contacts and two different rear designs (A = 4 cm^2) *= Measurements confirmed by Fraunhofer ISE Callab.

Rear design	V_{oc} [mV]	J_{sc} [mA/cm^2]	*FF* [%]	η [%]
Small BSF and large emitter area fraction	673	40.6	80.1	21.9*
Small BSF and small emitter area fraction	706	41.0	78.5	22.7*

Amorphous silicon hetero-junction

The HIT cells by Sanyo prove the excellent surface passivation quality of solar cells with hetero-junctions resulting in voltages of 743 mV on 98 µm thick n-type wafers [28].

At Fraunhofer ISE we have developed amorphous emitter and BSF structures using an Oxford cluster tool with PP and ICP PECVD chambers [29]. We are able to achieve voltages measured by SunsVoc [30] of 720 mV and 710 mV on flat and textured *n*-type wafers, respectively, with full-hetero front junction cells (see Figure 12, [31]). Such high V_{oc} values of more than 700 mV were also obtained on finished solar cells [29].

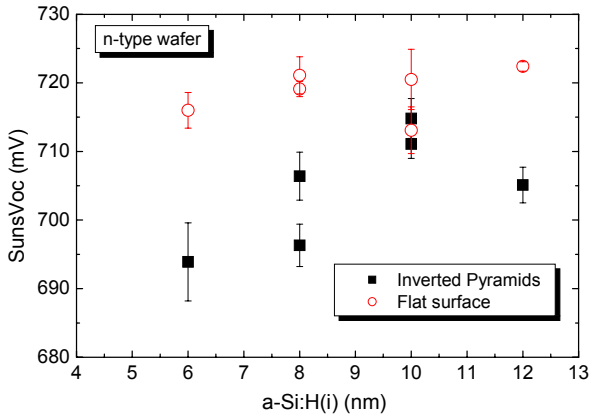

Figure 12 Open-circuit voltages of full hetero front junction cell precursors on flat and textured *n*-type silicon measured using the SunsVoc method.

Though it is possible to reach very high open-circuit voltages, a cell structure with front hetero-emitter is always a compromise between high voltage, good transport properties and blue response. Therefore our research will concentrate on interdigitated back contact hetero-junction solar cells. As a first step we have realized cells with hetero back junction and diffused front surface fields (Figure 13 and Table 5). Very encouraging results were obtained [32]. Unfortunately, on the textured n^+np^+ cells a technological problem with the metallization resulted in low *FF*s.

Table 5 Results of cells with back hetero-junctions and diffused FSF (A = 4 cm^2).

Cell structure	V_{oc} [mV]	J_{sc} [mA/cm^2]	*FF* [%]	η [%]
a) n^+np^+, flat	687	34.9	79.9	19.1
b) p^+pn^+, textured	667	37.8	78.6	19.8
c) n^+np^+, textured	681	37.8	*66.2*	*17.0*

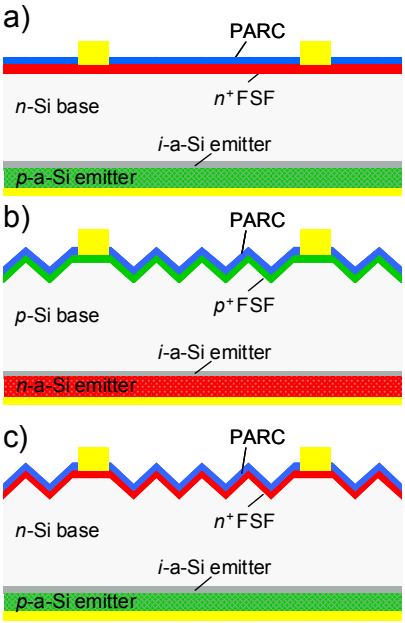

Figure 13 Hetero back junction cell structures with diffused front surface fields (FSF).

CONCLUSION

Our model calculations have shown that it is possible to reach an efficiency of around 20% on boron-doped oxygen-contaminated silicon with an industrially feasible cell structure. A main loss in such cells is the SRH recombination via the metastable boron-oxygen complex. Therefore for future cell generations, the material quality has to be increased. A very good choice would be *n*-type silicon which shows no light-induced degradation and is more tolerant to metal contaminations. However, the cell structure and process for *n*-type silicon has to be changed. It was shown that a variety of cell architectures with different efficiency potential and complexity are viable.

ACKNOWLEDGEMENT

The authors would like to thank J. Bartsch, N. Bayer, I. Druschke, A. Filipovic, F. Granek, S. Henneck, M. Hörteis, U. Jäger, N. Kohn, N. König, K. Krüger, A. Leimenstoll, C. Meinhardt, K.U. Ritzau, M. Reusch, M. Retzlaff, E. Schäffer, F. Schätzle, D. Schmidt, S. Seitz, J. Spannagel and K. Zimmermann. This work was supported by the German Federal Ministry for the Environment, Nature Conservation and Nuclear Safety under contract number 0329849A (Th-ETA).

REFERENCES

[1] H. Fischer and W. Pschunder, "Investigation of photon and thermal induced changes in silicon solar cells", *Proceedings of the 10th IEEE Photovoltaic Specialists Conference*, *Palo Alto, California, USA*, 1973, pp. 404-411.

[2] S. W. Glunz, S. Rein, J. Y. Lee, and W. Warta, "Minority carrier lifetime degradation in boron-doped Czochralski silicon", *Journal of Applied Physics 90*, 2001, pp. 2397-2404.
[3] J. Schmidt and K. Bothe, "Structure and transformation of the metastable boron- and oxygen-related defect center in crystalline silicon", *Physical Review B (Condensed Matter) 69*, 2004, pp. 0241071-0241078.
[4] D. Macdonald and L. J. Geerligs, "Recombination activity of interstitial iron and other transition metal point defects in p- and n-type crystalline silicon", *Applied Physics Letters 85*, 2004, pp. 4061-4063.
[5] A. W. Blakers, A. Wang, A. M. Milne, J. Zhao, and M. A. Green, "22.8% efficient silicon solar cell", *Applied Physics Letters 55*, 1989, pp. 1363-1365.
[6] E. Schneiderlöchner, R. Preu, R. Lüdemann, and S. W. Glunz, "Laser-fired rear contacts for crystalline silicon solar cells", *Progress in Photovoltaics: Research and Applications 10*, 2002, pp. 29-34.
[7] K. Bothe, R. Sinton, and J. Schmidt, "Fundamental boron-oxygen-related carrier lifetime limit in mono- and multicrystalline silicon", *Progress in Photovoltaics: Research and Applications 13*, 2005, pp. 287-296.
[8] M. J. Kerr and A. Cuevas, "General parameterization of Auger recombination in crystalline silicon", *Journal of Applied Physics 91*, 2002, pp. 2473-2480.
[9] O. Schultz, A. Mette, M. Hermle, and S. W. Glunz "Thermal oxidation for crystalline silicon solar cells exceeding 19% efficiency applying industrially feasible process technology", *Progress in Photovoltaics: Research and Applications 16*, 2008, pp. 317 - 324.
[10] D. Kray and S. W. Glunz, "Investigation of laser-fired rear-side recombination properties using an analytical model", *Progress in Photovoltaics: Research and Applications 14*, 2006, pp. 195-201.
[11] B. Fischer, "Loss analysis of crystalline silicon solar cells using photoconductance and quantum efficiency measurements", *PhD thesis,* Universität Konstanz, 2003.
[12] R. H. Cox and H. Strack, "Ohmic contacts for GaAs devices", *Solid State Electronics 10*, 1967, pp. 1213-1218.
[13] A. Wolf, D. Biro, A. Kimmerle, and R. Preu, *submitted for publication*, 2010.
[14] P. Saint-Cast, J. Benick, D. Kania, L. Weiss, M. Hofmann, J. Rentsch, R. Preu, and S. W. Glunz, "High-efficiency c-Si solar cells passivated with ALD and PECVD aluminum oxide", *IEEE Electron Device Letters*, 2010.
[15] P. Altermatt, S. Steingrube, Y. Yang, C. Sprodowski, T. Dezhdar, S. Koc, B. Veith, S. Herrman, R. Bock, K. Bothe, J. Schmidt, and R. Brendel, "Highly predictive modelling of entire Si solar cells for industrial applications", *Proceeding of the 24th European Photovoltaic Solar Energy Conference*, *Hamburg*, 2009, pp. 901-906.
[16] S. W. Glunz, S. Rein, J. Knobloch, W. Wettling, and T. Abe, "Comparison of boron- and gallium-doped p-type Czochralski silicon for photovoltaic application", *Progress in Photovoltaics: Research and Applications 7*, 1999, pp. 463-469.
[17] A. Herguth, G. Schubert, M. Kaes, and G. Hahn, "Avoiding boron-oxygen related degradation in highly boron doped Cz silicon", *Proceedings of the 21st European Photovoltaic Solar Energy Conference*, *Dresden, Germany*, 2006, pp. 530-537.
[18] B. Lim, S. Hermann, K. Bothe, J. Schmidt, and R. Brendel, "Permanent deactivation of the boron-oxygen recombination center in silicon solar cells", *Proceedings of the 23rd European Photovoltaic Solar Energy Conference*, *Valencia, Spain*, 2008, pp. 1018-1022.
[19] C. Schmiga et al., *to be published*, 2010.
[20] C. Schmiga, M. Hörteis, M. Rauer, K. Meyer, J. Lossen, H.-J. Krokoszinski, M. Hermle, and S. W. Glunz "Large-area n-type silicon solar cells with printed contacts and aluminium-alloyed rear emitter", *Proceedings of the 24th European Photovoltaic Solar Energy Conference*, *Hamburg, Germany*, 2009, pp. 1167-1170.
[21] M. Rauer, C. Schmiga, M. Hermle, and S. W. Glunz, "Passivation of screen-printed aluminium-alloyed emitters for back junction n-type silicon solar cells", *Proceedings of the 24th European Photovoltaic Solar Energy Conference*, *Hamburg, Germany*, 2009, pp. 1059-1062.
[22] J. Benick, B. Hoex, M. C. M. van de Sanden, W. M. M. Kessels, O. Schultz, and S. W. Glunz "High efficiency n-type Si solar cells on Al_2O_3-passivated boron emitters", *Applied Physics Letters 92*, 2008, pp. 253504/253501-253503.
[23] J. Benick, A. Richter, T. T. A. Li, N. Grant, K. R. McIntosh, Y. Ren, K. J. Weber, M. Hermle, and S. W. Glunz, "Changes in the Al_2O_3/Si interface properties due to a post-deposition anneal ", *this conference*, 2010.
[24] D. Suwito, U. Jäger, J. Benick, S. Janz, M. Hermle, and S. W. Glunz, "Industrially feasible rear passivation and contacting scheme for high-efficiency n-type solar cells yielding a V_{oc} of 700 mV", *IEEE Transaction of Electron Devices*, 2010.
[25] A. Richter, M. Hörteis, J. Benick, S. Henneck, M. Hermle, and S. W. Glunz, "Towards industrially feasible high-efficiency *n*-type Si solar cells with boron-diffused front side emitter – combining firing stable Al_2O_3 passivation and fine-line printing", *this conference*, 2010.
[26] D. De Ceuster, P. Cousins, D. Rose, D. Vicente, P. Tipones, and W. Mulligan, "Low Cost, high volume production of >22% efficiency silicon solar cells", *Proceedings of the 22nd European Photovoltaic Solar Energy Conference*, *Milan, Italy*, 2007, pp. 816-819.
[27] C. Reichel, M. Reusch, F. Granek, M. Hermle, and S. W. Glunz, "Decoupling charge carrier collection and metallization geometry of back-contacted back-junction silicon solar cells by using insulating thin films", *this conference*, 2010.
[28] M. Taguchi, Y. Tsunomura, H. Inoue, S. Taira, T. Nakashima, T. Baba, H. Sakata, and E. Maruyama, "High-efficiency HIT solar cell on thin (<100μm) silicon wafer", *Proceedings of the 24th European Photovoltaic Solar Energy Conference*, *Hamburg, Germany*, 2009, pp. 1690-1693.
[29] D. Pysch, C. Meinhardt, K. U. Ritzau, M. Bivour, K. Zimmermann, C. Schetter, M. Hermle, and S. W. Glunz, "Comparision of intrinsic amorpous silicon buffer layers for silicon heterojunction solar cells deposited by different PECVD techniques", *this conference*, 2010.
[30] R. A. Sinton and A. Cuevas, "A quasi-steady-state open-circuit voltage method for solar cell characterization", *Proceedings of the 16th European Photovoltaic Solar Energy Conference*, *Glasgow, UK*, 2000, pp. 1152-1155.
[31] D. Pysch et al., *to be presented at the EU-PVSEC*, *Valencia*, 2010.
[32] M. Bivour, C. Meinhardt, D. Pysch, C. Reichel, K. U. Ritzau, M. Hermle, and S. W. Glunz, "n-type silicon solar cells with amorphous/crystalline silicon heterojunction rear emitter", *this conference*, 2010.